Enhanced diffusion in smoothly modulated superlattices

Dmitry A. Rakhlin
Department of Physics, New York University, 4 Washington Place, New York, New York 10003
(Received 16 February 2000; revised manuscript received 13 September 2000; published 27 December 2000)

We investigate a superdiffusive behavior found in a quasiclassical model of a square-planar superlattice subjected to a perpendicular magnetic field. It is shown that certain accelerated domains are responsible for long trapping of tracers and setting them into near-ballistic motion. The mechanism of entrapment appears to be two-staged and multifractal. Relatively short trapping occurs in the vicinity of homoclinic tangles, created by intersections of stable and unstable manifolds of a hyperbolic fixed point, connected to itself. A structure of the quasitrap reveals families of multipulse solutions, doubly asymptotic to slow manifolds. The existence of orbits of this type was proved [G. Haller and S. Wiggins, Arch. Rational Mech. Anal. **130**, 25 (1995)] for integrable two-degree-of-freedom Hamiltonian systems with perturbation. We describe mixing dynamics in this region and examine characteristic escape time scales. More prolonged quasitrapping is due to sticking to resonant multilayered island chains that are found to accelerate ballistic transport. Phase-space dynamics is analyzed. We successfully employ a renewal process formalism to relate Poincare recurrences and coordinate variance asymptotics for both quasitraps and also justify the use of this formalism for the specific case of gradually increasing average velocity.

DOI: 10.1103/PhysRevE.63.011112 PACS number(s): 05.40.Fb, 05.45.Gg, 05.60.Cd, 66.30.−h

I. INTRODUCTION

In the last decade significant attention was brought to the investigation of so-called commensurability effects found in lateral surface superlattices (LSSL's) subjected to a magnetic field [1]. Commensurability appears in the interplay of superlattice period and Larmor radius. Other important parameters are the nature, geometry, and shape of lattice modulation as well as the time dependence and the geometry of the magnetic field. The interest to surface superlattices originates, primarily, from their nonlinear and nontrivial response to the applied magnetic field. Several interesting phenomena were observed [2,3], in particular, commensurability or Weiss oscillations of the longitudinal magnetoresistance found in bidirectionally (2DEG) strongly modulated superlattices [4]. Peaks in the magnetoresistance appeared for specific strengths of the magnetic field that would have caused unperturbed electrons to move along classical collision-free orbits encircling 1,2,4,9 . . . dots. Initially suggested ''pinned'' mechanism, which is well suited for the billiard model of reflecting disks, described experimental results quite closely. Two major flaws of this mechanism, noted in [5], are the assumption that circular cyclotron orbits do not respond to an electric field used to measure resistivity, and the failure to explain an additional peak in magnetoresistance which could not be associated with a collision-free orbit. This peak becomes predominant in samples of smaller electron densities. Later experiments on antidot LSSL's [6] revealed additional complexities in the behavior of the magnetoresistance. More peaks of varying intensity were observed, actual positions of peaks associated with collision-free orbits did not coincide with predicted ones. Having studied electron motion in phase space (x,y,v_x,v_y) by means of Poincare surfaces of section, the authors [5] concluded that peaks in magnetoresistance mainly are caused not by the varying number of pinned (regular) orbits within Kolmogorov, Arnold, and Moser (KAM) domains, but by correlations within the chaotic sea which also shows structure, reflecting the presence of nonlinear resonances. It has long been known, but not well understood, that boundaries of domains of regular motion can be ''sticky,'' meaning that chaotic trajectories can exhibit long stays near the boundaries in a narrow strip called the boundary layer. Chaotic trajectories, trapped in the layer, perform nearly regular motion for a long time, and thus, depending on the behavior of regular domain (oscillatory, accelerator, etc.), contribute to sub- or superdiffusive motion.

In this paper we consider the model of a 2DEG strongly smoothly modulated superlattice. We study an evolution of trapping structures within a chaotic sea and properties of their boundaries. Our results clearly demonstrate how a small variation of the model parameters can drastically change the pattern of chaotic electronic motion and how this change translates into the variation of macrotransport characteristics.

Our second goal is to present further analysis of a trapping mechanism which is realized in two-dimensional Hamiltonian systems and which is a plausible cause of the stickiness in resonant domains.

In a number of recent publications [7–9] it was suggested that at least in some cases the stickiness of a boundary layer is due to its specific substructure consisting of higher-order resonant islands surrounded by chaotic manifolds which connect fixed or periodic hyperbolic points. One example of a domain with such a structure of the boundary layer is an islands-around-island hierarchy studied in [10–12]. Most of its trapping time a tracer resides in the vicinity of the manifold that encircles a particular generation of islands. Transport across the hierarchy is realized as a sequence of jumps between intersecting turnstiles that belong to manifolds of neighboring generations. A similar scenario is observed in the case of trapping on a resonant multilayered island chains: manifolds now encircle different island layers, not generations.

The tracer dynamics within different types of chaotic hyperbolic manifold has been intensively studied in one-

dimensional (1D) area preserving systems with a perturbation (also known as $1\frac{1}{2}$ systems) [7,8,13]; few results are known for higher dimensional systems [14]. We were able to thoroughly analyze the chaotic dynamics in the vicinity of homoclinic tangles of 2D hyperbolic manifold. More importantly, the obtained results do not depend on the choice of a particular model. Indeed, for any two-dimensional Hamiltonian one of the angular variables is slow in the vicinity of a hyperbolic manifold. By a symplectic change of variables the Hamiltonian can be reduced to the resonant normal form which, for two degrees of freedom, is integrable. One can reduce it to a system with one degree of freedom depending on the constant value of the first integral as a parameter and then draw phase portraits. For a given resonance there are only finitely many types of phase portraits [15], and these types can be distinguished through the lowest-order terms in the normal form. The phase portraits are qualitatively distinct only for finitely many resonances. This allows us to extend the applicability of our observations to systems with the same type of phase portrait and, as discussed below, to some other 2D near-resonant systems.

The paper also discusses the problem of an adequate kinetic description for the *intermittent* motion found in systems with a sticky domain. Stickiness manifests itself in the slow polynomial decay of the number of particles in a bounded chaotic region of phase space that includes a sticky boundary layer: for large times this decay is best fitted by an algebraic law $N(t)\sim t^{-\nu}$. However, for a given system there might be no universal long-time behavior [11,16]. This fact is attributed to the coexistence of sticky structures with different time-scale characteristics such as accessibility time, transit time, etc. In this case their contributions in the transport asymptotics are significant in different time intervals. The problem of relating the local properties of sticky layers to macrotransport characteristics has been attacked by a number of techniques, such as Levy flights [17], continuous time random walks [18], renewal process formalism [19], fractional kinetics [10,12]. . . . However, we do not yet have good criteria to determine whether, or when, any of these techniques can be applied to a particular chaotic transport problem.

We have verified the set of necessary assumptions needed to justify the use of the renewal process formalism, which is based on a *one-flight approximation* method. Description of the method is given in Sec. IV. Using renewal process formalism, the global coordinate variance asymptotics were successfully related to long-time characteristics of local trapping structures. And the formalism was also generalized for the specific case of nonuniform velocity.

The article is organized as follows. Section II discusses the choice of a model, Sec. III is devoted to investigation of the main regimes of the model and the topology of the phase space. In Sec. IV we present the results of extensive computer simulation for averaged transport characteristics, analysis of the trapping in the vicinity of homoclinic hyperbolic manifolds, and the discussion of the statistics of multifractal intermittent motion found in our model.

II. MODEL HAMILTONIAN

From the quantum-mechanical point of view, electrons moving in a two-dimensional periodic potential with a square unit cell and subjected to a weak (or strong) magnetic field perpendicular to the plane of lattice, can be described by a tight-binding Harper model [20], which is valid in the one-band approximation. The spectrum of Harper's model was first computed by Hofstadter [21] and is commonly known as a Hofstadter butterfly. However, in the regime where the potentials of the magnetic field and the lattice are of comparable strength, the one-band approximation is not valid due to the coupling of Landau levels. The modified spectrum that accounts for coupling was recently computed in [22], and was shown to approach a continuous classical limit, i.e., many gaps are closed, Landau bands are merged and even weak disorder broadening, estimated in the self-consistent Born approximation, will close still open gaps.

The result is not surprising. Modulation-induced broadening of the Landau levels results in their overlapping, and this effect is known as magnetic breakdown. Magnetic breakdown allows electron transitions between states with different wave vectors that destroy both Bragg interference effects and size quantization within potential well regions. This justifies the choice of a classical Hamiltonian for the regime of strong coupling:

$$H(x,y,p_x,p_y)=\frac{1}{2m}\left[\left[p_x+\frac{eB}{2}y\right]^2+\left[p_y-\frac{eB}{2}x\right]^2\right]+V(x,y). \tag{2.1}$$

The crystalline potential is included by introducing the effective electron mass. The total energy is determined by the Fermi energy and $V(x,y)$ is the modulating potential. Depending on the preparation technique, $V(x,y)$ may be approximated by an egg-crate potential (smooth modulation)

$$V(x,y)=V_0\left[2+\cos\left(\frac{2\pi}{a}x\right)+\cos\left(\frac{2\pi}{a}y\right)\right] \tag{2.2}$$

or a steep antidot potential:

$$V(x,y)=V_0\left[\cos\left(\frac{2\pi}{a}x\right)\cos\left(\frac{2\pi}{a}y\right)\right]^{\beta} \tag{2.3}$$

with β characterizing the steepness of potential peaks.

Here we consider smooth modulation. The reason is twofold. On the one hand, a steep antidot potential can be represented by Sinai billiard, a model that has been studied intensively. On the other hand, smooth potential is advantageous for study of the enhanced ballistic transport. We expect that random scattering from the potential is a less relevant issue in smoothly modulated lattices. This assumption is based purely on practical considerations: the final step in process of preparation of steep antidot LSSL's is usually chemical wet etching, plasma etching, or damaging by irradiation. The rough surface of the reflecting cylinders will introduce strong scattering which impairs enhanced ballistic transport while allowing one to observe collision-free pinned

orbits. Smoothly modulated LSSL's can be realized by imposing the spatially distributed electric or magnetic field from highly doped gates or an array of superconductors lying atop the structure and separated by insulator layer, thus allowing more smooth variation. The scattering on impurities is another issue relevant to both smoothly modulated and antidot lattices. We will discuss this matter below.

Measuring the energy and length in Eqs. (2.1) and (2.2) in units of the potential strength and lattice constant, respectively, we obtain the dimensionless Hamiltonian:

$$H(x,y,p_x,p_y)=\frac{1}{2}[p_x+\lambda y]^2+\frac{1}{2}[p_y-\lambda x]^2+V(x,y) \tag{2.4}$$

with scaled potential

$$V(x,y)=2+\cos x+\cos y. \tag{2.5}$$

The dimensionless quantity

$$\lambda=\frac{eB\,a}{4\pi\,(mV_0)^{1/2}}=\frac{\omega_c}{2\omega_0} \tag{2.6}$$

describes the strength of the nonintegrable coupling between two degrees of freedom due to the magnetic field. Lambda and the total energy are the only two parameters defining the behavior of the system.

Introducing the velocities

$$v_x=p_x+\lambda y, \quad v_y=p_y-\lambda x \tag{2.7}$$

one can obtain the equations of motion in the following form:

$$\begin{aligned} \dot{x}&=v_x, \quad \dot{v}_x=\sin x+2\lambda v_y, \\ \dot{y}&=v_y, \quad \dot{v}_y=\sin y-2\lambda v_x. \end{aligned} \tag{2.8}$$

Note that variables v_x, x and v_y, y are not canonical. The Hamiltonian in these variables can be written as

$$H(x,y,v_x,v_y)=\frac{v_x^2}{2}+\frac{v_y^2}{2}+2+\cos x+\cos y. \tag{2.9}$$

The introduction of noncanonical variables is justified by the convenience of choosing an ''elementary cell'' in the phase space: the Hamiltonian and equations of motion written are symmetrical with respect to translations along x and y by $2\pi n$. One can identify, therefore, coordinates mod(2π) and reduce them to the unit cell $[0,2\pi]$. Velocities are limited within some interval defined by the total energy. Thus, the choice of noncanonical variables allows one to get a compact Poincare section. We will be calling components of energy: $E_i=v_i^2/2+\cos(i)+1$, $i=x,y$ the ''*energy of i pendulum.*'' Energy exchange between X and Y pendulums is possible only if the magnetic field is nonzero.

The model described by Eq. (2.8), (2.9) was introduced in [23]. Earlier work [24] considers the superposition of potentials (2.2) and (2.3) with no magnetic field as a simple nonintegrable model of two interacting pendulums. In the low-interaction regime, the authors [24] found a transition from one-dimensional channeling to two-dimensional diffusive motion, this effect was called stochastic percolation. Essentially the same effect was found in the model (2.8), (2.9) [23]. It was also pointed out in [24] that in certain energy intervals the transport is anomalous.

We will briefly describe the features of the model in the low coupling regime (a detailed analysis can be found in [23]) and will concentrate mostly on newly found bifurcations that change the topology of KAM domains, as well as properties of their boundary layers. Bifurcations occur at the relatively high energies: $E=3.1-3.6$, $\lambda=0.15$. Simple estimation shows that the classical model is still valid within this range of parameters. Indeed, the measure for the strength of the coupling of Landau bands can be written [22] as $K=2\pi ma^2V_0/h^2$. Then one can estimate

$$\frac{E_f}{\hbar\omega_c}=\frac{1}{\lambda}\frac{a}{\lambda_f}\frac{(2\cdot E)^{1/2}}{4}\simeq 30 \tag{2.10}$$

for typical values of $a/\lambda_f=8-10$. We also have that

$$K\frac{\Phi_0}{\Phi}=\frac{2\pi ma^2V_0}{h^2}\frac{h/eB}{a^2}=\frac{V_0}{\hbar\omega_c}\simeq 10, \tag{2.11}$$

where Φ_0/Φ is the ratio of the magnetic flux quantum to the flux through a unit cell. As one easily can obtain the normalized magnetic flux to be close to one, the parameter K appears to be large. At these values of the Fermi energy, the coupling strength, and the magnetic flux, the energy spectrum will approach a continuous limit (see Fig. 3 in [22]).

III. MAIN REGIMES, DOUBLING BIFURCATIONS

The potential V in Eq. (2.5) has minima at the energy $E=0$, saddle point at $E=2$, and maxima at $E=4$. Depending on the total energy, we distinguish three energy regimes. In the *low-energy* regime $E<2$, all orbits are localized within one unit cell near the potential minima for all values of λ. For *intermediate energies* $2<E<4$, drifting quasiperiodic orbits extended in the X but not in the Y direction, or vice versa, may coexist with localized orbits. At *high energies* $E>4$, the possible orbits are, in principle, not restricted in configuration space. In the intermediate regime and at high values of the coupling parameter ($\lambda\sim 0.1$–0.3, depending on total energy) the invariant domains corresponding to delocalized regular motion, disappear. This is another difference between the cases of a smooth and a steep antidot potential. In the latter case, particles follow circular trajectories between collisions and the existence of such special orbits as circular, rosette, drifting, ... depends purely on the strength of the magnetic field. A smooth potential provides effective energy exchange between pendulums, making possible the simultaneous presence of a variety of orbit types in the corresponding range of parameters. Apparently, these orbits are not regular, therefore enhanced or suppressed diffusion will persist only in the presence of ''anomalous'' structures which are able to entrap tracers for a long time.

We found such well-defined structure at a specific set of

parameters $E_f=3.325$, $\lambda=0.15$. The formation of this structure is two-staged, being a result of two doubling bifurcations. The first bifurcation is observed at $E_f=3.18$, $\lambda=0.15$. In place of a central elliptical point, two elliptical points of period two and saddle are formed [Fig. 1(a)]. With a further increase of energy the KAM tori, which surround the separatrix, are transformed into cantori chains, which eventually merge with the chaotic sea. At about $E_f=3.31$, $\lambda=0.15$, the last resonant island chain reaches the chaotic sea and the saddle point splits with the formation of a central elliptic point and two saddle points of period two [Fig. 1(b)]. In this figure the next stage can be seen: as the energy goes higher the cantori chains located within the regular domains of side elliptical points reach inner boundary of broken separatrix and form boundary island chains. Magnification of these multilayered island chains is depicted in Fig. 7. At the energy $E\simeq 3.6$, $\lambda=0.15$ the last KAM tori in these regions ceases to exist and the side elliptical points collapse [Fig. 1(c)].

Below we will concentrate on the regime $E=3.325$, $\lambda=0.15$ which presents the two aforementioned structures serving as quasitraps: the *''outer''* quasitrap is located in the vicinity of separatrix that separates regular domain around the central elliptical point and chaotic sea. The *''inner''* quasitrap is formed by multilayered island chains contained within side separatrice loops. These islands encircle side domains of regular motion. While within quasitraps, a particle does not gain enough energy to jump in the Y direction, it moves ballistically along X. A corresponding X quasitrap, that disallows the motion in the X direction can be seen in Fig. 1(b) at the upper and lower boundaries of the stochastic sea.

The Y quasitrap rotates almost undeformed with period two, e.g., revolution by 2π in the V_yY plane correspond to shift on 4π along the X direction. The Poincare section presented in Fig. 1(d) is taken at $x=2\pi$, $x=\mathrm{mod}(2\pi)$, instead of $x=\pi$, compared with previous sections. The corresponding rotation of the Y quasitrap is $\pi/2$.

To demonstrate the impact of Y and X quasitraps on the pattern of random motion, we have examined Levy walks in the XY plane for the regimes before the second bifurcation: $E_f=3.30$, $\lambda=0.15$ [Fig. 2(a)], after the second bifurcation: $E_f=3.325$, $\lambda=0.15$ [Fig. 2(b)], and beyond the third bifurcation: $E_f=3.6$, $\lambda=0.15$ [Fig. 2(c)]. The Poincare section on Fig. 2(c) has one elliptic point; side elliptic points have collapsed. Long walks, shown in Fig. 2(b) correspond to ballistic flights of the particle confined within an X or Y quasitrap.

IV. MACROSCOPICAL TRANSPORT CHARACTERISTICS

In order to estimate the influence of the quasitraps we have performed several numerical experiments including the measurement of coordinate variances (Fig. 3), of the Poincare recurrences distribution (Fig. 4), and of the escape time distribution (Fig. 5). Except for the measurements of the escape time distribution, the averaging was performed over 2×10^3 trajectories in a time interval of about 10^6 revolutions. Initial conditions for this set were chosen within the chaotic sea, outside of quasitraps, in the region of localized motion.

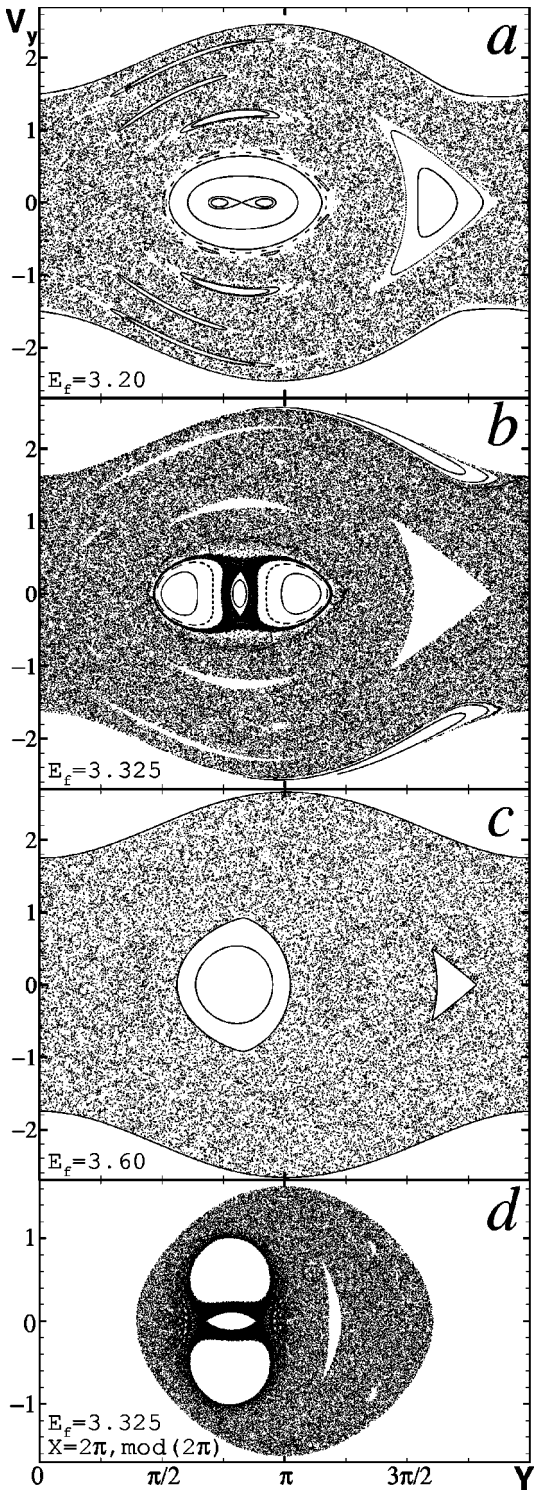

FIG. 1. Bifurcations. Coupling paramater $\lambda=0.15$. (a) formation of a hyperbolic fixed point at $E_f=3.18$, (b) the separatrix splits and merges with the chaotic sea at $E_f=3.31$, (c) side elliptical points collapse at $E\simeq 3.6$, (d) rotation of the 8-shaped separatrix in V_yY plane.

Since the period of revolution varies in different regions of the Poincare section, it is not a convenient characteristic of motion. The step of integrator is a more natural time variable here as it naturally relates velocity and position: Δt

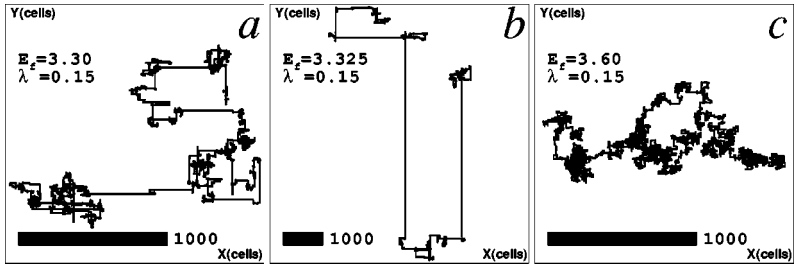

FIG. 2. Levy walks of a tracer on XY plane for three different regimes: (a) before the second bifurcation, (b) after the second bifurcation, (c) beyond the third bifurcation. The distance is measured in unit cells (equal to 2π); the scale is the same for X and Y direction and is indicated for each plot. Initial coordinates of the tracer ($X=\pi$, $Y=1.0$, $V_y=0.0$), and the time of computation (2.5×10^6 steps of integrator) are the same for all three plots. Total path lengths are quite close: 9.4×10^4, 10^5, and 1.2×10^5 cells.

$=|\Delta\vec{r}|/|\vec{v}|$. A rough scale for the trajectories within the Y quasitrap is 23–25 steps/period.

The analysis of distributions yields the following results:

(i) Direct measurement of the coordinate variance versus time allows one to estimate the exponent μ, for $\langle(r-\langle r\rangle^2)\rangle\sim t^{\mu}$, $1\leqslant\mu\leqslant2$. Linear extrapolation of the curve depicted in Fig. 3(a) gives $\mu=1.7$ in the interval $10^{3.5}$–$10^{5.3}$ steps or, roughly, 10^2–10^4 revolutions and $\mu=1.9$ in the time interval $10^{6.1}$–$10^{6.9}$ steps [Fig. 3(b)]. Beyond $10^{6.9}$ steps μ monotonically decreases up to 1.4; we will discuss this effect below.

(ii) Poincare recurrence distribution $\Phi(t)\sim t^{-\gamma}$ (Fig. 4) also shows different exponents: $\gamma=2.1$ in the time interval $10^{4.6}-10^{5.3}$ steps [Fig. 4(b)] and $\gamma=3.8$ in the time interval $10^{6.1}$–$10^{6.9}$ steps [Fig. 4(c)].

(iii) To deduce the exit time distribution exponent ν, $\Psi(t)\sim t^{-\nu}$, we have chosen another three sets of initial coordinates, the first two having 3×10^4 points and the last one

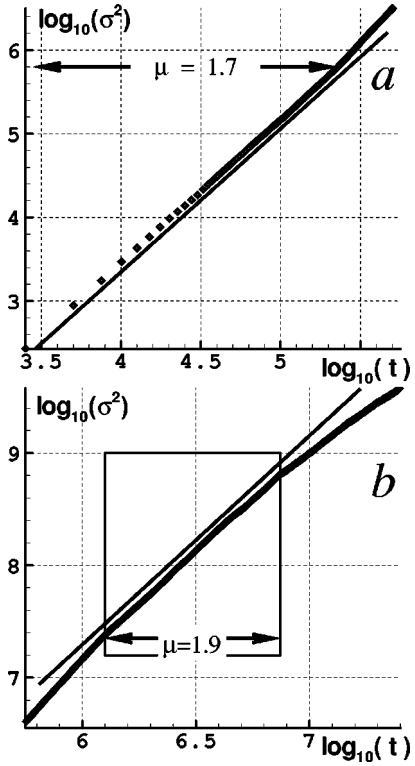

FIG. 3. Coordinate variance $\sigma^2=\langle(r-\langle r\rangle)^2\rangle$ has its asymptotics proportional to t^{μ}; μ can be different in different time intervals. Distance is measured in unit cells (equal to 2π), time is measured in steps of integrator. $E_f=3.325$, $\lambda=0.15$. The averaging is performed over 2×10^3 trajectories during 2.5×10^7 steps (about 10^6 revolutions).

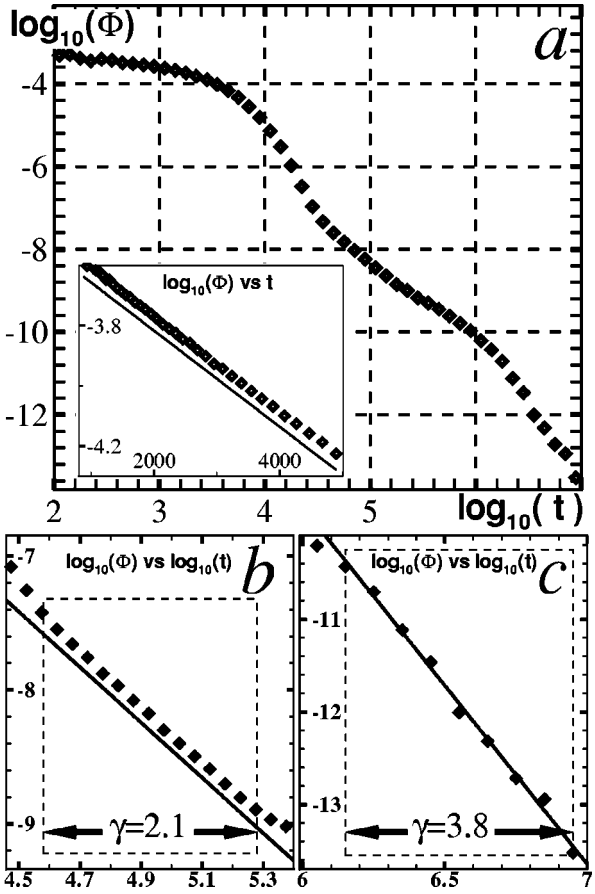

FIG. 4. Poincare recurrence distribution also has different power asymptotics: $\Phi(t)\sim t^{-\gamma}$. (a) full distribution, (b) linear approximation of the short-time asymptote, $\gamma=2.1$, (c) linear approximation of the long-time asymptote, $\gamma=3.8$. The inset in (a) shows exponential decay of the distribution up to $10^{3.7}$ steps. $E_f=3.325$, $\lambda=0.15$. The averaging is performed over 2×10^3 trajectories during 2.5×10^7 steps (about 10^6 revolutions). Initial conditions were chosen within the region of chaotic localized motion.

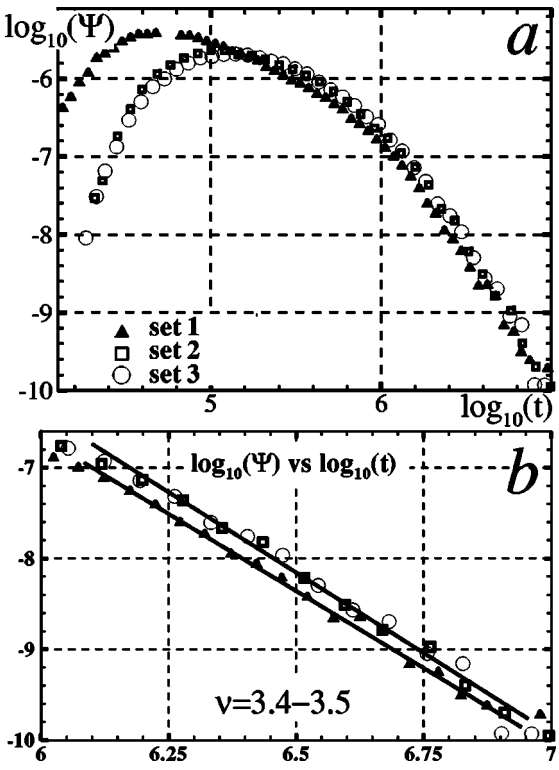

FIG. 5. Escape time distribution for three sets of initial points. Set 1: $Y\in[2.575,2.6]$, $V_y\in[0.33,0.35]$, 3×10^4 points. Set 2: $Y\in[2.74,2.76]$, $V_y\in[0.0,0.1]$, 3×10^4 points. Set 3: $Y\in[2.76,2.78]$, $V_y\in[0.01,0.09]$, 4×10^4 points. (a) full distribution. (b) linear approximation of the long-time asymptote $\Psi(t)\sim t^{-\nu}$, $\nu=3.4-3.5$. $E_f=3.325$, $\lambda=0.15$.

having 4×10^4 points. The initial points of the first set were located at the outer boundary of separatrix in the vicinity of the saddle point, within the interval $[2.575,2.600]$ along Y and within $[0.33,0.35]$ along V_y on the Poincare section $x=\pi$, $x=\mathrm{mod}(2\pi)$. Initial points of the second set were chosen within separatrix loops, but away from multilayered islands (inner quasitrap): $Y\in[2.74,2.76]$, $V_y\in[0.0,0.1]$. The last set covered an area $[2.76,2.78]\times[0.01,0.09]$ that lies in the vicinity of the first (closest to separatrix) island chain. Figure 7 shows the locations of these sets. Simulation continued until all points left the Y quasitrap. For the time interval $10^{6.1}$–$10^{6.9}$ steps, ν was found to be equal 3.5 for the second and the third sets, and 3.4 for the first one. The error of estimation is of order 0.1, which makes it reasonable to suggest equal asymptotics for all three sets. Figure 5 presents the escape time distributions for all three sets.

Further analysis proved that different ''short-time'' and ''long-time'' behavior are caused by the sticking to outer and inner quasitraps. One may wonder, why are we fitting the power laws on small intervals of data and distinguishing two sets of asymptotics? The reason is that the inner and outer quasitraps are different in a sense that a variation of the model parameters changes their trapping properties and topology independently. There is no renormalization group between these two quasitraps, and therefore observed asymptotic variations are not the log-periodic corrections to some ''averaged'' asymptote, introduction of which would be meaningful for a renormalizable structure. (See, for example, the study of trapping in the islands-around-island hierarchy [16]). The next two subsections demonstrate that short- and long-time asymptotics reflect individual trapping properties of two different quasitraps.

A. Analysis of short-time sticking

The results of the simulations show that short-time sticking occurs in the vicinity of a separatrix, shown in white on the density plot (Fig. 6). The magnified fragment of Fig. 6 is depicted in Fig. 7.

An underlying structure that controls the dynamics in the vicinity of a separatrix is two homoclinic tangles, created by the intersections of stable and unstable manifolds of a hyperbolic periodic (period two) point connected to itself. Two consecutive primary intersections of the manifolds define a lobe, and the lobes are responsible for the flux through the resonance. The resonance condition implies that the corresponding angular frequencies admit a nontrivial integer combination which vanishes on some domain of the phase space. In such cases one can apply a symplectic change of variables which transforms the resonant combination of the phase variables into a new angle variable which slowly varies in the neighborhood of the resonant domain. The evolution of a system, which has two different time scales in some localized domain, can be conventionally analyzed using a single perturbation technique:

$$\dot I=-\epsilon D_\phi H_1(x,I,\phi;\epsilon),$$
$$\dot\phi=D_I H_0(x,I)+\epsilon D_I H_1(x,I,\phi;\epsilon), \tag{4.1}$$

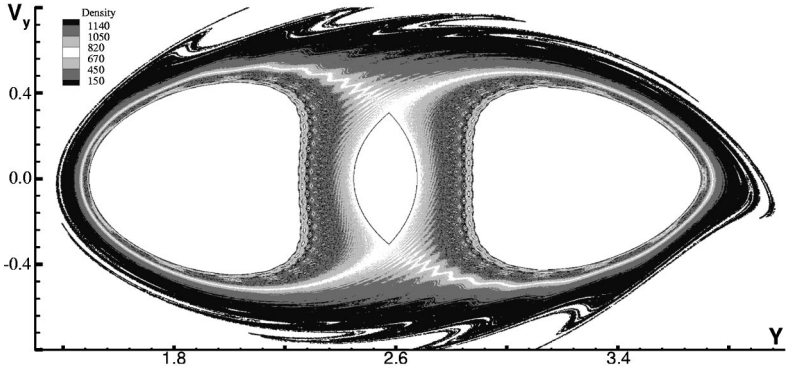

FIG. 6. Density of trajectories within Y quasitrap. $E_f=3.325$, $\lambda=0.15$. 10^3 initial points were taken in the region of multilayered island chains. Simulation continued until all trajectories left the box $(1.2,4.0)\cdot(-0.8,0.8)$. The number of hits in each pixel of size $0.002\cdot0.002$ is color coded according to the legend. The maximum density is observed within the inner quasi-trap–the hierarchy of multilayered island chains. (See magnified fragment of this structure in Fig. 7). Maximum number of hits in 1581. Resolution is 1400 by 800.

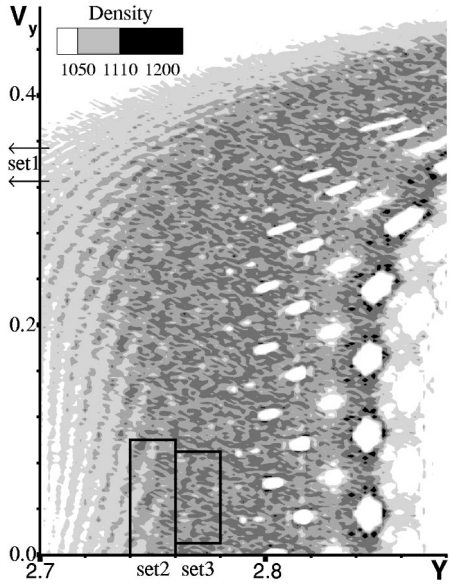

FIG. 7. The distribution of trajectory density within multilayered island chains. Magnified fragment of Fig. 6 .

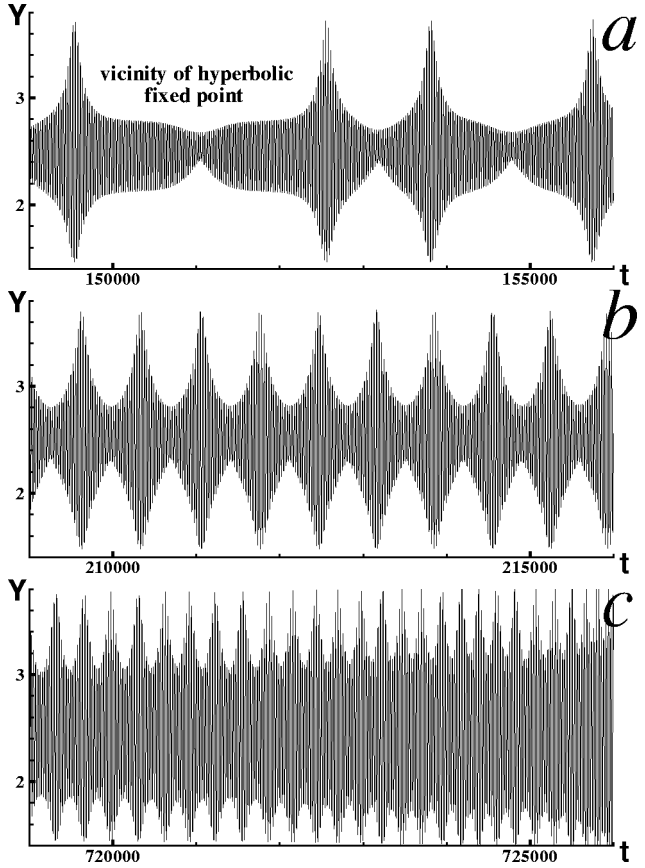

FIG. 8. Trapped coordinate as a function of time for the single trajectory exiting from the *Y* quasitrap. $E_f = 3.325$, $\lambda = 0.15$. Initial coordinates: (2.83, 0.225) (vicinity of the third island chain) (a) wandering in the vicinity of the separatrix. (b) trajectory goes back to islands. (c) trajectory exits the quasitrap. Time is measured in steps of integrator.

where H_0 is the Hamiltonian of unperturbed system, ϵH_1 is the perturbation, periodic in variable ϕ.

A well-known example of the application of such a technique is a whisker map, which is defined to be the leading-order approximation in ϵ and H to the separatrix map. The separatrix map was introduced in [25] and was shown to have peculiar properties such as a hidden renormalization group [13,14] and *n*-step periodic solutions [7,26]. Expansion around these solutions revealed the existence of local areas of stability, which were called *tangle* islands. Though it is correct in its description of some general properties, the separatrix map approximation falls short in its prediction of long-time characteristics of near-separatrix motion, as the map parameters quickly deviate from those of the original system.

Recently the *energy-phase method* was developed [8], which provides a criterion for proving the existence of multipulse homoclinic orbits near hyperbolic-resonant, two degree of freedom Hamiltonian systems, which spend time of order $\log_{10}(1/\epsilon)$ near the slow manifold on which the resonance occurs. These are orbits negatively asymptotic to some invariant set in the hyperbolic invariant manifold A_ϵ which enter and leave a small neighborhood of A_ϵ of order $O(\epsilon^{1/2})$ N_ϵ times, then finally return and approach the invariant set of A_ϵ asymptotically. The number of times an orbit approaches and leaves this neighborhood depends on the *phase shift* along the slow manifold which, in turn, depends on parameter of perturbation ϵ. The distribution of the number of pulses as a function of the phase shift is fairly stable at low N_ϵ and becomes increasingly sensitive to small changes in the parameters for higher number of pulses. This puts the limit of order $O(1/\epsilon^{1/2})$ on the total passage time: following an individual orbit numerically beyond this limit is extremely difficult. In the 2D system where the perturbation is ''self-induced,'' the phase shift along the trajectory varies, making the spectrum of N_ϵ-pulse orbits ''continuous.'' Sensitivity to a small change in the parameters also means that the problem of finding the asymptotic behavior of trajectories becomes a singular perturbation problem. Nonetheless, it can be addressed from the different viewpoint that utilizes the *fibering* of the stable and unstable manifolds by submanifolds consisting of initial trajectories that have the same ''asymptotic phase,'' meaning these trajectories asymptote to the same orbit in $A_{\epsilon=0}$. Fibering allows one to view the problem as a regular perturbation one. It was shown [27] that fibers perturb smoothly in $\epsilon^{1/2}$ and $O(\epsilon^{1/2})$ close to unperturbed fibers. Fibers are invariant under the flow, i.e., fibers are mapped into fibers. This kind of solution is not amenable to Melnikov-type methods.

Our model is two-dimensional and is more complex for the analysis than the one studied in [8,27]. Primarily this is due to the fact that the perturbation is changing on the slow time scale. Nonetheless, the behavior of individual orbits in the vicinity of slow manifolds is still similar to one observed in $1\frac{1}{2}$ system. To demonstrate this we have performed two series of numerical simulations.

We have analyzed the pattern of motion of the trajectory that originates from multilayered islands located within separatrix loops, crosses the separatrix and exits from the quasi-

trap (Fig. 8). Two conclusions can be drawn. First: motion in this region is highly correlated and can be represented by a modulated periodic function of period 4π as the period doubles; the period of modulation tends to infinity as the trajectory approaches the hyperbolic invariant manifold. The period of modulation and the period of regular oscillations can be considered the two time scales that are used in the perturbative analysis. As the trajectory approaches the outer boundary of the quasitrap, the periodicity of modulation degrades, and finally, the modulation disappears. The second conclusion is that the trajectory indeed approaches and leaves the vicinity of the invariant manifold several times before it finally exits.

In terms of perturbative analysis the estimations of ϵ led us to the following. An unperturbed system can be viewed as two coupled pendulums involved in resonance energy exchange: in the vicinity of the saddle points the energy of the *X* pendulum oscillates periodically between 3.325 and 2.855 with period 4π, and the energy of the *Y* pendulum oscillates in the range 0.0–0.47 also with the period 4π. Total energy is conserved and equal to 3.325. As expected, the amplitude of the energy exchange is proportional to λ: $0.47/3.325 \simeq 0.15$. On a Poincare section $x=2\pi$ unperturbed oscillations of the *Y* pendulum would be represented by an invariant curve containing hyperbolic points of the perturbed system. The last invariant tori corresponding to the resonant energy exchange between pendulums existed at $E_f=3.31, \lambda=0.15$: it separated the separatrix from the external chaotic sea. Thus, the upper boundary for ϵ can be estimated as $3.325-3.31=0.015$, or about 0.5% of the total energy.

The second series of numerical experiments demonstrates the existence of fibers around the separatrix and displays their evolution. In this series we used two sets of initial conditions, located within the area $\Delta Y \cdot \Delta V_y=(2.86,3.12)(-0.3,0.0)$ on Poincare section $x=2\pi$, $x=\mathrm{mod}(2\pi)$ that includes part of the stable manifold and its vicinity near the hyperbolic fixed point. The 3.7×10^5 initial conditions in the first (ordered) set were placed on the knots of the net of the size $n\times m=N_{set}$, while 10^5 points in the second (random) set were distributed randomly and uniformly over the same area. The trajectories for the ordered set were computed over 10^4 steps, and trajectories for the random set were computed over $10^{5.3}$ steps.

Figure 9(a) exhibits a deformation of the random set along the 2D homoclinic manifold. *X* coordinate of consecutive mappings differs by 2π. We defined T_{fast} as a period of time needed to cover this distance. Thus, Fig. 9(a) presents evolution of the set after 55, 85, and 115 T_{fast}. Study of the set evolution allowed us to draw the following conclusions:

(a) The set stretches around the manifold forming a spiral. The spiral does not self-intersect, its length grows with time.

(b) Consecutive mappings of the set are ''enclosed'': they do not intersect each other.

(c) Minimal distance between the spiral and the hyperbolic point decreases with time.

(d) Neighboring points stay close the for quite a few revolutions around the separatrix: the fine texture of (overlapping) mappings shown in Fig. 9(b) lasts about 1000 steps or $(1-5)T_{slow}$, where T_{slow} is a period of time needed to com-

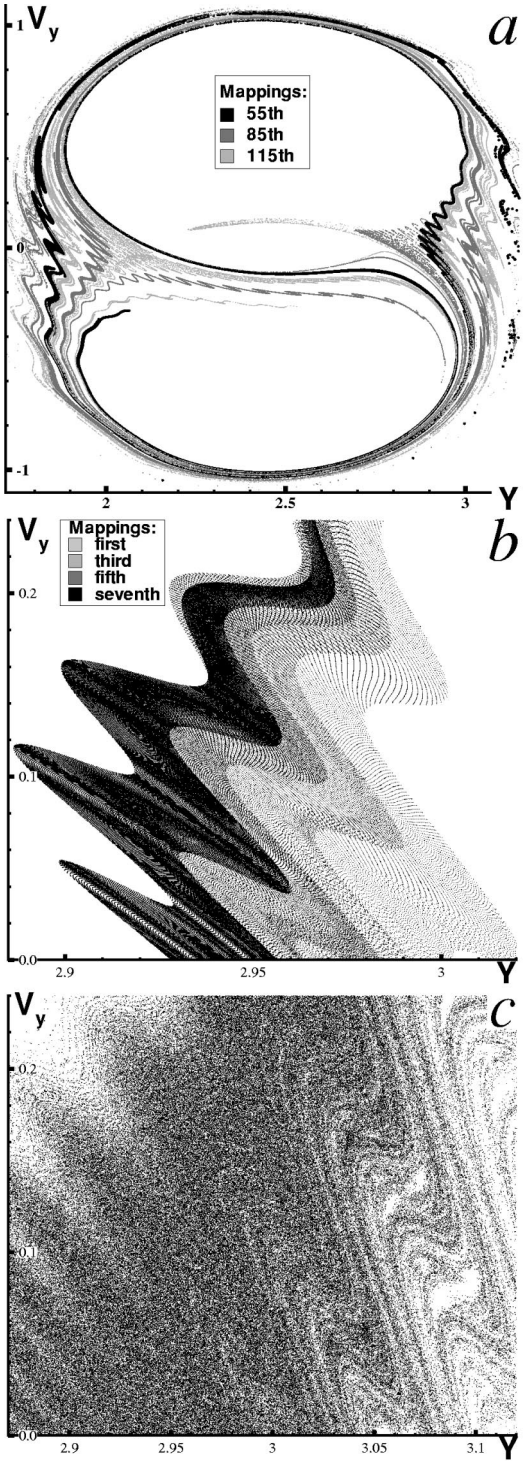

FIG. 9. The deformations of two sets of points along the 2D stable manifold. (a) three mappings of 10^5 points from the ''random'' set. *X* coordinate of two consecutive mappings differs by 2π. (b) magnified fragments of four (overlapping) mappings of 3.7×10^5 points from the ''ordered'' set during their first passage around the separatrix. Fine texture of mappings lasts about $(1-5)T_{slow}$ (10^3 steps). In order to see this texture in the monochrome picture, mappings 1–7 depict every 7th, 5th, 3d, all trajectories respectively. (c) distribution of the points from the ''ordered'' set after 10^4 steps. Poincare sections (a)–(c) are taken at $X=2\pi$, $E_f=3.325$, $\lambda=0.15$.

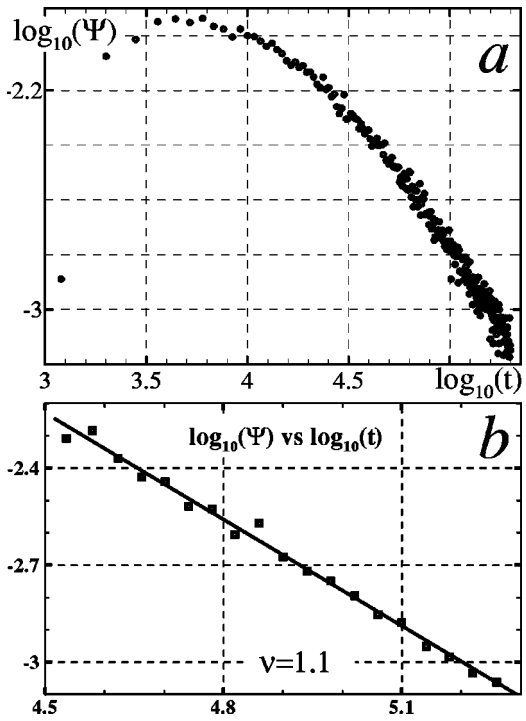

FIG. 10. Escape time distribution for the second (random) set of 10^5 points trapped in the vicinity of the separatrix. Initial coordinates were uniformly distributed within the area $Y \in [2.87,3.12]$, $V_y \in [0.0,-0.3]$, $X=2\pi$. (a) full distribution, (b) linear approximation of the short-time asymptote $\Psi(t) \sim t^{-\nu}$, $\nu=1.1$. Time is measured in steps of integrator. $E_f=3.325$, $\lambda=0.15$.

plete a revolution around the separatrix. Longer T_{slow} is measured closer to the separatrix. The fine texture also indicates clearly the regions of extensive stretching.

The corollary of statements (a)–(d) is that any set of points in the vicinity of the separatrix deforms to a spiral. Different sets form spirals which, at a given time, can have different widths, lengths, and different ''averaged'' positions on the separatrix. The longer the spiral the closer its ''outer'' end to the boundary of the quasitrap. For an exiting trajectory at the boundary, T_{slow} and T_{fast} are of the same order.

Mappings of the set which contains all points from the $\epsilon^{1/2}$ vicinity of the separatrix were called fibers in the earlier publications [9,27]. We have shown that fibers are shaped as spirals, and they are doubly asymptotic to the separatrix. Fibers can map on each other, but they do not intersect.

Thin fiber structure is visible until about 5×10^3 steps for the random set and at least until 10^4 steps for the ordered set [Fig. 9(c)]. (We did not compute the evolution of the ordered set beyond 10^4 steps). The mixing time in the quasitrap coincides with the maximum of the exit time distribution (Fig. 10). By that time only a small percentage of trajectories leaves the quasitrap. We attribute the greater mixing time in the ordered set to the existence of internal resonances reflecting the initial ordering of points. Polynomial long-time asymptotic for the random set is well defined in the interval $10^{4.5}$–$10^{5.3}$ steps and equal to 1.1. This agrees very well with Poincare recurrences asymptotic for the short-time trapping [Fig. 4(b)]. In the same interval of time γ was found to be equal to 2.1. The relationship $\nu=\gamma-1$ is discussed below. Our estimation of the escape time for the random set ($10^{3.7} \simeq 5000$ steps) agrees well with the Poincare recurrences distribution [see inset in Fig. 4(a)]: at times shorter than $10^{3.7}$, the distribution is purely exponential. Since the initial conditions for the Poincare recurrences distribution were taken outside of the quasitrap, the exponential part consists of those points which were not trapped at all. Observed escape time $10^{3.7}$ steps approximately equal to $200T_{fast} \simeq (1/\epsilon)T_{fast}$. The average T_{slow} for both sets was about 430 steps or $16T_{fast}$. Thus, the escape time is also approximately $(1/\epsilon^{1/2})T_{slow}$, where $\epsilon=5\times10^{-3}$. Notice, however, that the period of slow motion varies significantly with the distance from the separatrix. The difference in T_{slow} across the whole quasitrap is a least an order in magnitude—from about 10^3 to less than 10^2 steps.

B. Analysis of trapping statistics

To relate the exponent γ for the Poincare recurrence distribution to μ, where $\langle (r-\langle r\rangle)^2\rangle \sim t^{\mu}$ we employ a *renewal process formalism*, one of the methods describing the *one-flight approximation* [19,28]. The formalism is based on the use of the velocity autocorrelation function

$$C(t)=\langle \mathbf{v}(t)\cdot\mathbf{v}(0)\rangle = 2\langle v_x(t)v_x(0)\rangle, \tag{4.2}$$

of random walker which performs statistically independent free paths moving with a constant velocity v_0. The durations T of these paths are distributed as $\Psi(T)\sim T^{-\gamma}$, where $\Psi(T)$ is the probability density function. Results are applicable for $T \gg T_{local}$, where T_{local} is the characteristic duration of the localized motion. In the second equality in Eq. (4.2) we have used the square symmetry of our system and the fact that free paths of duration T in negative or positive directions have equal probability. $\langle\ \rangle$ represents time averaging.

We briefly outline the derivation of this formalism as we will need modify it for the case of nonconstant velocity, described in the next section. Assumptions about tracers' behavior are met in our setup, since trajectories for the Poincare recurrence distribution start and end up in the phase volume, located outside of quasitraps, and the motion in this volume is localized. Thus, the long flights occurring in the vicinity of the separatrix can be deemed statistically independent. The span of flight durations ($10^{3.7}$–$10^{5.3}$) is much greater than the average time of localized motion, which is of order 10^{2-3} steps. Although a tracer trapped in the vicinity of the separatrix does not move with uniform speed, it is sufficient to use its average velocity as v_0. Indeed, the velocity in the vicinity of the separatrix can be approximated by a modulated periodic function with period much smaller than the minimum flight duration at which out random walker formalism is valid. The period of modulation is infinite on the separatrix, and decreases at the periphery of the quasitrap. However, as we have roughly an equal number of flight crossing (or reflecting back from) the separatrix from both sides, one can introduce an average amplitude of the velocity. The reason why we expect equal influx from both sides, is that the characteristic transit time through the outer

quasitrap is much less than that through the inner one. Equivalently, the probability that a trajectory which penetrated the outer quasitrap from outside will reenter it again, is much higher than the probability that it will be trapped on the inner quasitrap.

The flight of duration T along X gives the following contribution to the correlation function:

$$C(t) \sim \int_0^\infty v(t+\tau)v(\tau)d\tau = \int_0^{T-t} v(t+\tau)v(\tau)d\tau = v_0^2(T-t), \tag{4.3}$$

which simply manifests that for $t \leqslant T$ the contribution of this single path to $C(t)$ is proportional to the length of the interval in which the correlation between time τ and $\tau+t$ is possible.

Using probability density function for the flight duration distribution and normalizing the correlation function one obtains

$$C(t) = \frac{v_0^2}{\langle T \rangle} \int_T^\infty (T-t)\Phi(T)dT, \tag{4.4}$$

where the statistical independence of flights has been used.

Only single paths between 0 and t contribute to the correlation function above. The word ''single'' is used for paths that consist of the following three phases: wandering in the chaotic sea outside of a quasitrap within the region of localized motion, correlated motion in a certain direction within a quasitrap, wandering in the chaotic sea again.

Complex flights consisting of two or more paths have an equal probability of ending up with positive or negative speed and do not contribute (for more details, see [28]). Generally, this assumption does not work for the case of gradually increasing velocity, considered in the next section. Nonetheless, one can still resort on the argument that for a given total flight duration, a single flight is more probable. Indeed, if for large T the probability of being trapped once is proportional to $T^{-\gamma}$, then the probability to reenter the quasitrap decays as $\int_0^t \tau^{-\gamma}(t-\tau)^{-\gamma}d\tau \sim t^{-2\gamma+1}$.

In addition we have used the following technique to disregard complex flights: since there is no clear boundary between the chaotic sea and the outer quasitrap, we have assumed the flight is single, if it does not reenter the box that includes this quasitrap, and that part of the chaotic sea where the direction of motion is the same as in the quasitrap. In the assumption above, such a flight can be qualified as single.

Denoting the Laplace transforms of $C(t)$ and $\Phi(T)$ by $\tilde{C}(s)$ and $\tilde{\Phi}(s)$, Eq. (4.4) turns into

$$\tilde{C}(s) \sim \frac{1}{s} + \frac{1}{\langle T \rangle} \frac{\tilde{\Phi}(s)-1}{s^2}. \tag{4.5}$$

Using the relationship between the mean-square displacement and correlation function:

$$\sigma^2(t) = 2\int_0^t (t-\tau)C(\tau)d\tau, \tag{4.6}$$

whose Laplace transform is $\widetilde{\sigma^2}(s) = 2s^{-2}\tilde{C}(s)$, one can get

$$\sigma^2(t) = 2\mathbf{L}^{-1}\{s^{-3} + \langle T \rangle^{-1} s^{-4}[\tilde{\Phi}(s)-1]\}, \tag{4.7}$$

where $\mathbf{L}^{-1}$ is the inverse Laplace transform. To obtain long-time asymptotics one should consider small s behavior. For the case of interest $2<\gamma<3$, the calculations yield: $\sigma^2(t) \sim t^{4-\gamma}$ or $\mu+\gamma=4$.

For intermediate asymptotics in the time interval $10^{4.6}$–$10^{5.3}$ steps, corresponding to trapping in the vicinity of the separatrix, we have obtained $\gamma+\mu=2.1+1.7=3.8$, which agrees well with the one-flight approximation.

We emphasize again, that the obtained relationship between μ and γ is not a unique result of the outlined formalism. This result was first derived in [29] under a different initial formulation and restrictions. Later there were developed ''jump'' [18] and ''velocity'' [30] versions of the continuous-time random-walk description. Though both versions produced the same relationship between μ and γ, the jump version was found deficient in its description of velocity power spectrum asymptotics. The ''velocity'' model was later generalized to allow the velocity to vary from flight to flight, according to a given probability density function [31]. The reason for the use of the renewal process formalism is that its assumptions can be adequately justified. The formalism can also be easily generalized to be applied to the specific case of nonuniform velocity, as is done in the next section.

C. Transport across multilayered island chains

Long flights, contributing to the tail of the distribution, reside mostly on the *inner* quasitrap—that is what we have called the hierarchy of multilayered islands, surrounding two side elliptic points. Figure 7 shows a close-up view of this structure with five well-defined layers, the sixth is destroyed. Each layer has the same number of islands, the first, second, and fourth layers have a self-similar subisland hierarchy. Figure 7 demonstrates that, except for the aforementioned hierarchical structures, the inner quasi-trap is almost uniformly dense, providing long trapping times. Trapping on hierarchical structures of the fourth chain is a possible reason for low density at the last (fifth) layer. After a careful examination we have concluded that characteristic accessibility times to the higher generations of islands in hierarchical structures are larger than the time of our computations. An indication of this can be seen on Fig. 3(b): the exponent μ for a coordinate variance asymptotic decreases monotonically beyond 10^7 steps either to a new value or to one, that is the case if the accessibility time to a second generation is higher and all other sources of effective trapping are depleted. Asymptotics obtained for time less than 10^7 steps, are not therefore affected by the presence of self-similar structures, and we can exclude these structures from consideration.

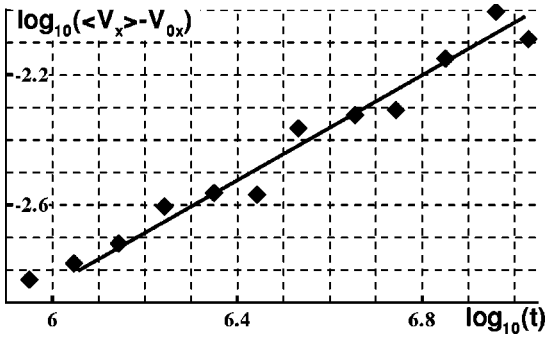

FIG. 11. Average velocity of tracers within multilayered island chains as a function of trapping time. The dependence is assumed to be in the form $\langle V_x\rangle = V_{0x} + aT^{\alpha}$, $\alpha = 0.80 \pm 0.05$. Averaging was performed over 10^3 trajectories.

For quasitrapping on island chains, the exponents γ and μ for escape time distribution and coordinate variance can be related in a similar way, shown in the previous section. However, we can no longer assume a constant velocity of tracers as we did above. The velocity is still a modulated periodic function. But its amplitude, averaged over the period of modulation, increases as the tracer penetrates deeper into island layers. Given the fact that stickiness across the inner quasitrap is almost uniform, one can suggest that longer flights penetrate deeper toward the most inner island chain. Thus, we expect longer flights to have higher average velocity. Figure 11 presents the correlation of the average velocity with the flight length. To relate the growth of the average velocity to the properties of islands, one has to make certain assumptions about the transition rates between island chains and their scaling properties. We were puzzled by the peculiar grouping of points on Fig. 11 and have verified that each group of points corresponds to the trapping on particular island chain. One must admit, though, that observed polynomial growth can result from averaging over many contributing factors, not the least of which might be a multifractal behavior of individual islands within chains.

For now we simply use the result presented in Fig. 11 and set that $v \sim v_0 t^{\alpha}$, $\alpha = 0.80 \pm 0.05$. Then the contribution of flight duration T will be

$$C(t) \sim v_0^2 \int_0^{T-t} \tau^{\alpha} (t+\tau)^{\alpha} d\tau = \frac{v_0^2}{1+\alpha} T^{\alpha} (T-t)^{1+\alpha} {}_2F_1\left(-\alpha, 1, 2+\alpha, 1-\frac{t}{T}\right). \tag{4.8}$$

${}_2F_1(\,)$ is the hypergeometric function.

The reasoning is exactly the same as when calculating the contribution of a single flight in the case of constant speed. The expression above converges anywhere on the circle $t \leqslant T$. Above we were able to obtain Laplace transform of the correlation function without specifying the explicit form of the flight distribution function. This time we have to reverse this order to simplify our task. We assume the same form of escape time distribution as was used in the original derivation of the renewal process formalism [32]: $\Phi(T) = A(B + CT)^{-\gamma}$, with normalization $AB^{1-\gamma}/C(\gamma - 1) = 1$. For simplicity we assume $B = C = 1$, $A = \gamma - 1$. Thus,

$$C(t) = \frac{v_0^2 A}{\langle T\rangle (1+\alpha)} \int_t^{\infty} T^{\alpha} (T-t)^{1-\alpha} \times {}_2F_1\left(-\alpha, 1, 2+\alpha, 1-\frac{t}{T}\right) (1+T)^{-\gamma} dT. \tag{4.9}$$

After a few algebraic transformations this integral can be taken by parts, yielding

$$C(t) = \frac{v_0^2 A}{\langle T\rangle} \frac{\Gamma(1+\alpha)\Gamma(-2-2\alpha+\gamma)}{(\gamma-1)\Gamma(-1-\alpha+\gamma)} t^{1+2\alpha} (1+t)^{1-\gamma} \times {}_2F_1\left(1+\alpha, -1+\gamma, -1-\alpha+\gamma, \frac{1}{1+t}\right) \tag{4.10}$$

valid if $(\gamma - 2\alpha) > 2$. The variance can still be written in the form (4.6). After performing the integration and taking the limit $t \to \infty$

$$\sigma^2(t\to\infty) = \frac{2v_0^2 A}{\langle T\rangle} \begin{cases} \dfrac{\Gamma(1+\alpha)\Gamma(-4-2\alpha+\gamma)}{(\gamma-1)\Gamma(-1-\alpha+\gamma)} t^{4+2\alpha-\gamma}, & 2+2\alpha < \gamma < 3+2\alpha \\ -\dfrac{\Gamma(2+2\alpha)\Gamma(-3-2\alpha+\gamma)}{(1+\alpha)\Gamma(\gamma)} t, & 3+2\alpha < \gamma. \end{cases} \tag{4.11}$$

At $\alpha = 0$ the formula reduces to the result of the previous section.

In the time interval 10^6–$10^{6.9}$ steps, where we associate with the quasitrapping on the sticky layers of island chains, we have $\mu = 1.90 \pm 0.05$, $\gamma = 3.75 \pm 0.1$, $\nu = (3.4 - 3.5) \pm 0.1$, depending on the set and $\alpha = 0.80 \pm 0.05$. Thus, the relationship $\mu = 4 + 2\alpha - \gamma = 4 + 1.6 - 3.75 = 1.85$ satisfies this.

At this point we have to explain the difference between Poincare recurrence and escape time asymptotics. Below is an excerpt from the work of Meiss [33]. According to the author the exit time probability distribution for the entry set I is the probability that a trajectory in I will have a given exit

time:

$$\mathrm{Prob}(t^+(I)=j)=\frac{\mu(T_j)}{\mu(I)}, \tag{4.12}$$

where $t^+(I)=t_{A\to M\setminus A}(I)$ is exit time, $A\subset M$ and $I\subset A$ is the *incoming* set with backward exit time 1. T_j is part of the incoming set with exit time j. If set A is chosen so that the characteristic *transit* time for it is much longer than the characteristic *accessibility* time of the entry set of A from some subset of $M\setminus A$, then the asymptotic for escape time for entry set must be equivalent to the asymptotic γ for the Poincare recurrences distribution for that subset of $M\setminus A$.

For the *accessible* set $A_{acc}\subset A$

$$\mathrm{Prob}(t^+(A_{acc})=k)=\frac{1}{\mu(A_{acc})}\sum_{j=k}^{\infty}\mu(T_j), \tag{4.13}$$

which is the same as the survival probability for I up to normalization. Similarly the transit time probability is

$$\mathrm{Prob}(t_{transit}(A_{acc})=j)=\frac{1}{\mu(A_{acc})}\sum_{k=0}^{j-1}\mu(T_j)=j\frac{\mu(T_j)}{\mu(A_{acc})}. \tag{4.14}$$

These equations imply that if $\mu(T_k)\sim k^{-\beta}$, $\beta>2$, as $k\to\infty$, then

$$\begin{aligned}\mathrm{Prob}(t^+(I)=k)&\sim k^{-\beta}\\ \mathrm{Prob}(t^+(I)\geqslant k)&\sim\mathrm{Prob}(t^+(A_{acc})=k)\\ &\sim\mathrm{Prob}(t_{transit}(A_{acc})=k)\\ &\sim k^{-(\beta-1)},\end{aligned} \tag{4.15}$$

which means that $\nu=\gamma-1$ for escape from the accessible set. The same result under a different approach was obtained in [34]. Our measurements of escape time and Poincare recurrence asymptotics for the trapping in the outer quasitrap confirm this relationship: $\gamma=2.1$ and $\nu=1.1$. In the case of the inner quasitrap, however, $\gamma=3.75\pm0.1$ and $\nu=(3.4-3.5)\pm0.1$ (e.g., ν varies between 3.4 and 3.5 for different sets and the precision is of order 0.1). The explanation is as follows. For the outer quasitrap the characteristic mixing time ($10^{3.7}$ steps for the random set which was used to compute the escape time distribution) is less than the minimum time at which the polynomial decay begins. Thus, we have computed the escape time distribution for the accessible set, which is the whole quasitrap. This is not true for the inner quasitrap: the mixing time is much greater there and therefore the escape time distribution was computed for small subsets $s_i\subset A_{acc}$. In this case it is easy to see that

(1) if all points of s_i belong to different trajectories that start on the incoming set, AND

(2) if the span between the shortest and the longest time intervals needed to reach points of s_i from the incoming set (accessibility time) is much less than the characteristic time at which the asymptotic behavior $t^{-\gamma}$ is observed, then the escape time asymptotic for set s_i is equal to γ. Violation of the first condition means that one counts a single trajectory several times. This would lead to an asymptotics less than γ and, in the limit $s_i\equiv A_{acc}$, would produce an asymptotic $\gamma-1$. Violation of the second condition would produce a greater asymptotic as one fails to account for long pieces of the trajectories. The particular choice of subsets s_i suggests that the second condition is being held as all three sets are located within the outer quasitrap where the transit time is known and is much less than that for the inner quasitrap. The first condition is violated, probably because all subsets s_i were initially ordered. The previous section demonstrates how the ordering affects the escape time statistics. That would explain the departure of obtained escape time asymptotics from γ or $\gamma-1$.

V. CONCLUSION

The fine structure of the stochastic layer was always a problem of great interest and became more significant as the problem of anomalous transport in dynamical chaos arose for different applications. In this paper we have analyzed the phase-space dynamics in the vicinity of two-dimensional hyperbolic slow manifolds. This structure is thought to be responsible for the long trapping in islands-around-island hierarchies and multilayered resonant island chains (the layers of the whiskered hyperbolic tori created in the destruction of resonant KAM tori in nearly integrable Hamiltonian systems). A general global perturbation theory for such structures does not currently exist even for one-dimensional systems. A rigorous analysis of two-dimensional Hamiltonian systems is trickier because the ''self-induced'' perturbation generally have a wide Fourier spectrum.

We have shown that in a particular model trajectories in the vicinity of the slow manifold form a hierarchy of thin submanifolds known as fibers. We have shown that fibers are shaped as spirals, and that they are doubly asymptotic to the slow manifold. Fibers map on each other, but do not intersect.

Generally, the observed picture coincides with the one predicted for $1\frac{1}{2}$ systems [27]. We have shown that the characteristic trapping time in the vicinity of the slow homoclinic manifold is about $(1/\epsilon)\cdot T_{fast}$ (period of perturbation) and $(1/\epsilon^{1/2})\langle T_{slow}\rangle$, where $\langle T_{slow}\rangle$ is the averaged period of slow motion around the separatrix. The width of the quasitrap and, consequently, the variation of T_{slow} within it are much bigger than those assumed in the earlier studies of low-dimensional systems [8,27]. We estimate that for an exiting trajectory at the boundary of the quasitrap, T_{slow} and T_{fast} are of the same order. Further study is needed to verify the dependence of the trapping time on ϵ for different values of perturbation.

As was discussed in the introduction, the results obtained for our model are applicable to other 2D systems with a similar type of resonance. Another fact allows us to suggest even broader applicability: our simulations show that the near-separatrix orbit dynamics observed in our model is similar to one predicted for lower dimensional systems. However, in terms of the topology of the phase space, the original studies of one-dimensional Hamiltonian systems as-

sumed only the existence of a resonant homoclinic manifolds [8,27]. It implies that any 2D near-resonance Hamiltonian, whose reduced 1D counterpart has a homoclinic structure, might exhibit similar phase-space dynamics in the vicinity of resonant manifolds.

We have concluded that renewal process formalism can be applied to the case of a velocity that is not constant during the flight, but rather oscillates around the median with an average period of oscillations much less than the duration of the flight. This is not surprising, though, because the average velocity is limited within a certain interval defined by the total energy and by the location of the quasitrap, and for any given flight length only nonsymmetry in the probability distribution function for an average velocity would affect the coordinate variance asymptotic. This would be, however, a higher-order correction.

We have shown that macrotransport characteristics of LSSL's are indeed highly susceptible to small changes in parameters and that this effect is related to the existence and the evolution of trapping structures within the chaotic sea. Practically, our model can be realized and long flights can be detected, at least those with length up to 10^2–10^3 unit cells, corresponding to the trapping in the vicinity of the separatrix. The usual technique that can be applied is the analysis of the velocity power spectrum, which can be directly obtained from measurements of conductivity $\sigma(\omega)$ in the far-infrared and microwave range. Anomalous regimes will be reflected by a power-law increase as $\omega \to 0$, which will hold up to crossover frequency $\omega_{cr} \sim 1/\tau_{coll}$, defined by the scattering on impurities. The upper limit of the power-law regime is given by the harmonic frequency ω_0 of the superlattice potential. In pure systems with mobilities in the range 10^6 cm^2/V s crossover frequency is of the order of $\omega_{cr} \sim 3 \times 10^{10}$ [35,36]. A typical carrier density $N \sim 2 \times 10^{11}$ cm^{-2} corresponds to $E_f = 10$ meV. To reproduce the regime studied in our model, one has to make the modulation potential of order $V_0 = 3$ meV. Corresponding harmonic frequency $\omega_0 = (2\pi/a)(V_0/m)^{1/2} \sim 3 \times 10^{12}$ for $a = 200$ nm. The magnetic field which corresponds to $\lambda = 0.15$ is $B \sim 0.5T$. This simple estimation yields a modest span of order 10^2 cells. There is evidence, however, that for chaotic systems with finite-size quasitraps, the effective lower limit crossover frequency is, actually, lower than $1/\tau_{coll}$ because the mobility is limited primarily by small-angle scattering which may or may not oust a particle from a quasitrap. In experiments [37] on magnetoconductance fluctuations in ballistic microstructures, which were shaped as a stadium and a circle, a long polynomial tail in the power spectrum for the circle persisted up to lengths of at least an order more than the measured free path length. The authors in a later study of the effects of random noise on magnetoresistance [38] demonstrated that in some ranges of parameters scattering does not destroy the polynomial tail. Their model of random noise, however, could not fit the experimental data [37]; it either killed the polynomial tail at a high level of noise or gave a significantly slower decrease in the exponential part of the spectrum. This disagreement is probably an indication of prevailing small-angle scattering in the experimental system.

ACKNOWLEDGMENTS

This work was supported by the U.S. Department of Energy, Grant No. DE-FG02-92ER54184. Computations were performed on SP2 supercomputer clusters at the University of San Diego and at the University of Michigan. We thank NPACI for providing the computer time. The author would like to personally thank George Zaslavsky for his guidance and numerous discussions.

[1] Recent theoretical reviews: R. Menne and R. R. Gerhardts, Phys. Rev. B **57**, 1707 (1998); J. Kučera, P. Středa, and R. R. Gerhardts, *ibid.* **55**, 14 439 (1997); Experimental articles: X. Wu, *ibid.* **56**, 15 744 (1997); O. Yevtushenko and K. Richter, *ibid.* **57**, 14 839 (1998).

[2] R. R. Gerhardts, D. Weiss, K. Klitzing, Phys. Rev. Lett. **62**, 1173 (1989).

[3] R. Schuster *et al.*, Phys. Rev. B **50**, 8090 (1994); M. Hayne, A. Usher, J. J. Harris, and C. T. Foxon, *ibid.* **56**, 10 446 (1997); G. Berthold, J. Smoliner, V. Rosskopf, E. Gornik, G. Böhm, and G. Weinmann, *ibid.* **66**, 11 350 (1992).

[4] D. Weiss. M. L. Roukes, A. Menschig, P. Grambow, K. Klitzing, and G. Weimann, Phys. Rev. Lett. **66**, 2790 (1991).

[5] R. Fleischmann, T. Geisel, and R. Ketzmerick, Phys. Rev. Lett. **68**, 1367 (1992).

[6] E. Vasiliadou, R. Fleischmann, D. Weiss, D. Heitmann, K. v. Klitzing, T. Geisel, R. Bergmann, H. Schweizer, and C. T. Foxon, Phys. Rev. B **52**, 8658 (1995); R. Schuster *et al.*, *ibid.* **50**, 8090 (1994).

[7] V. Rom-Kedar and G. M. Zaslavsky, Chaos **9**, 697 (1999).

[8] G. Haller and S. Wiggins, Arch. Rational Mech. Anal. **130**, 25 (1995).

[9] S. Wiggins, *Global Dynamics, Phase Space Transport, Orbits Homoclinic to Resonances and Applications* (AMS, Providence, RI, 1993).

[10] G. M. Zaslavsky, M. Edelman, and B. A. Niyazov, Chaos **7**, 159 (1997).

[11] R. B. White, S. Benkadda, S. Kassibrakis, and G. M. Zaslavsky, Chaos **8**, 757 (1998).

[12] A. I. Saichev and G. M. Zaslavsky, Chaos **7**, 753 (1997).

[13] G. M. Zaslavsky and S. S. Abdullaev, Phys. Rev. E **51**, 3901 (1995).

[14] L. I. Kuznetsov and G. M. Zaslavsky, Phys. Rep. **288**, 457 (1997).

[15] V. I. Arnold, V. V. Kozlov, and A. I. Neishtadt, *Dynamical Systems*, in Encyclopedia of Mathematical Sciences Vol. 3 (Springer-Verlag, Berlin, 1993).

[16] S. Benkadda, S. Kassibrakis, R. B. White, and G. M. Zaslavsky, Phys. Rev. E **59**, 3761 (1999).

[17] E. W. Montroll and M. F. Shlesinger, in *Studies in Statistical Mechanics* (North-Holland, Amsterdam, 1984), Vol. 11, p. 1.

[18] M. F. Shlesinger, B. J. West, and J. Klafter, Phys. Rev. Lett. **59**, 1100 (1987); M. F. Shlesinger and J. Klafter, *ibid.* **54**, 2551 (1985).

[19] T. Geizel, A. Zacherl, and G. Radons, Phys. Rev. Lett. **59**, 2503 (1987); T. Geizel, A. Zacherl, and G. Radons, Z. Phys. B: Condens. Matter **71**, 117 (1988).
[20] P. G. Harper, Proc. R. Soc. London, Ser. A **68**, 874 (1955).
[21] D. R. Hofstadter, Phys. Rev. B **14**, 2239 (1976).
[22] D. Springsguth, R. Ketzmerick, and T. Geisel, Phys. Rev. B **56**, 2036 (1997).
[23] J. Wahgenhuber, T. Geisel, P. Niebauer, and G. Obermair, Phys. Rev. B **45**, 4372 (1992).
[24] D. K. Chaikovsky and G. M. Zaslavsky, Chaos **1**, 463 (1991).
[25] G. M. Zaslavsky and N. N. Filonenko, Zh. Éksp. Teor. Fiz. **52**, 1281 (1967) [Sov. Phys. JETP **25**, 851 (1967)].
[26] G. M. Zaslavsky and M. Edelman, Chaos **10** (1), 135 (2000).
[27] N. Fenichel, J. Diff. Eqs. **31**, 53 (1979).
[28] T. Geisel, in *Levy Flights and Related Topics in Physics* (Springer, New York, 1995), p. 153.
[29] C. F. F. Karney, Physica D **8**, 360 (1983).
[30] G. Zumofen and J. Klafter, Phys. Rev. E **47**, 851 (1993); G. Zumofen and J. Klafter, Physica D **69**, 436 (1993).
[31] E. Barkai and J. Klafter, in *Chaos, Kinetics, and Nonlinear Dynamics and Fluids and Plasmas* (Springer, New York, 1998), p. 373.
[32] T. Geisel and S. Thomae, Phys. Rev. Lett. **52**, 1936 (1984).
[33] J. D. Meiss, Chaos **7**, 139 (1997).
[34] G. Zumofen and J. Klafter, Phys. Rev. E **59**, 3756 (1999).
[35] E. Vasiliadou, R. Fleischmann, D. Weiss, D. Heitmann, K. v. Klitzing, T. Geisel, R. Bergmann, H. Schweizer, and C. T. Foxon, Phys. Rev. B **52**, 8658 (1995).
[36] G. Berthold, J. Smoliner, V. Rosskopf, E. Gornik, G. Bvhm, and G. Weimann, Phys. Rev. B **45**, 11 350 (1992).
[37] C. M. Marcus, A. J. Rimberg, R. M. Westervelt, P. F. Hopkins, and A. C. Gossard, Phys. Rev. Lett. **69**, 506 (1992).
[38] W. A. Lin, J. B. Delos, and R. V. Jensen, Chaos **3**, 655 (1993).